Supporting Information

Interface Electron Polarization based High-*k* Al_2O_3/ZnO Nanolaminates with Excellent Temperature Stability and Ultrahigh Energy-storage Density by Atomic Layer Deposition

*Jin Li, Maowen Liu and Xiaofang Bi**

Key Laboratory of Aerospace Materials and Performance (Ministry of Education), School of Materials Science and Engineering, Beihang University (BUAA), Beijing, 100191, China

***Corresponding Author**

E-mail: bixf@buaa.edu.cn; Phone: +86-10-82339231

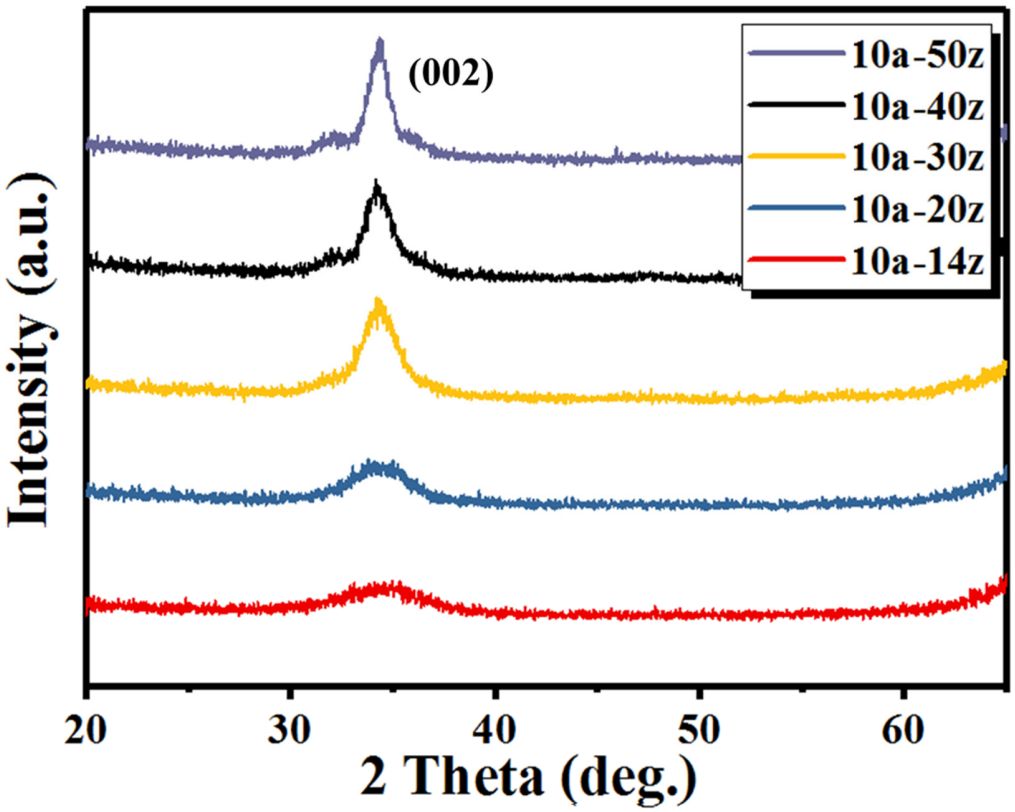

Figure S1. X-ray diffraction patterns of the AZ-NLs with W_{ZnO} varying from 50 to 14 cycles.

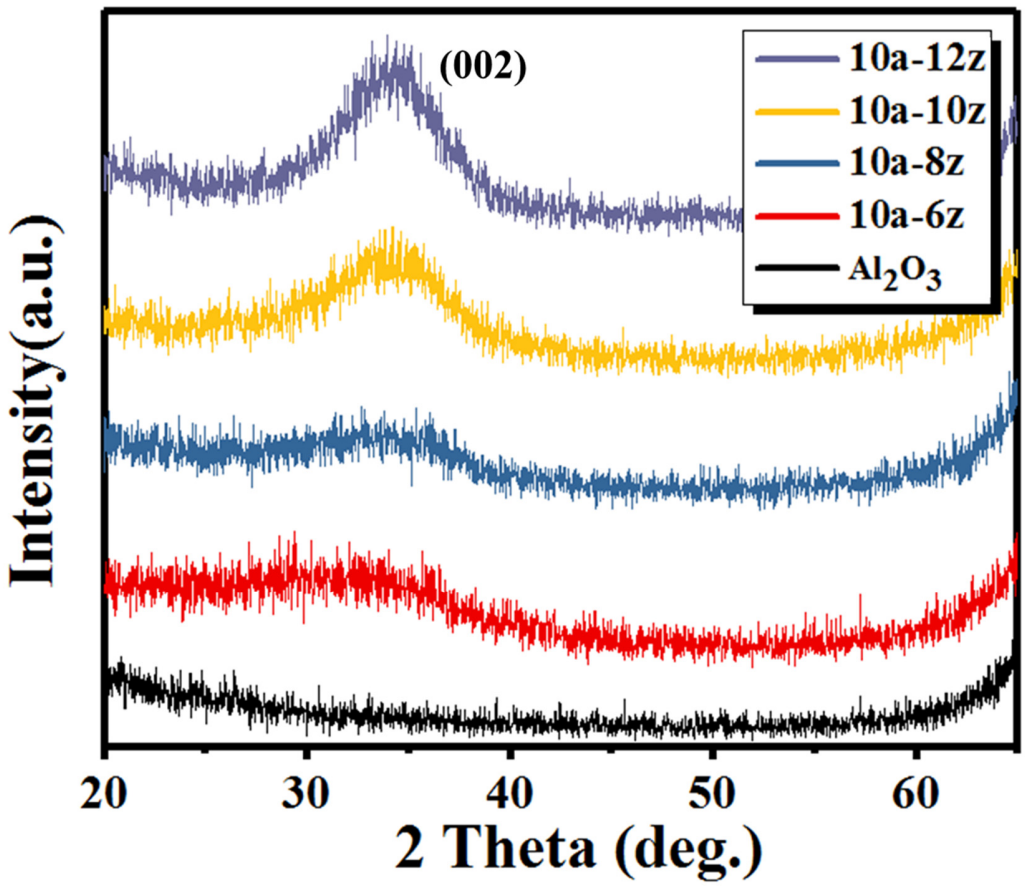

Figure S2. X-ray diffraction patterns of the AZ-NLs with W_{ZnO} varying from 12 to 6 cycles, together with that of Al_2O_3 single film for comparison.

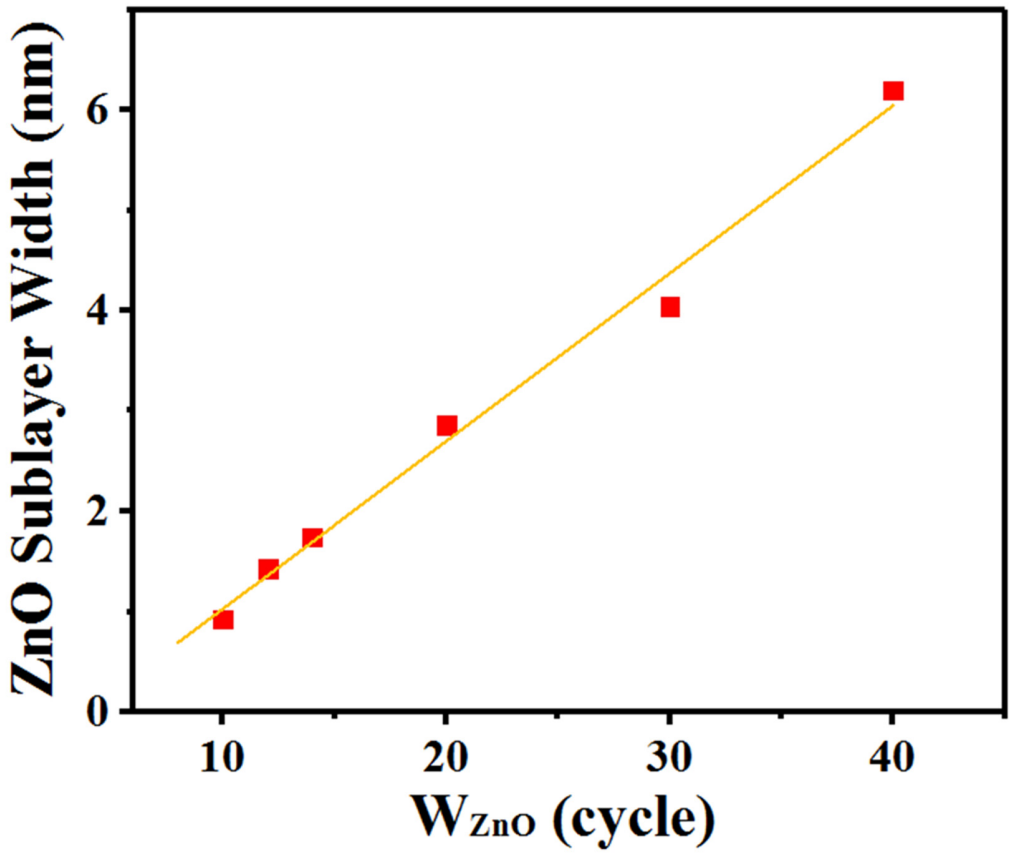

Figure S3. The ZnO sublayer width in AZ-NLs as a function of W_{ZnO}, while W_{Al2O3} is fixed at 10 cycles. A growth rate of 1.7Å per cycle is obtained for ZnO from the slope of the fitted straight line.

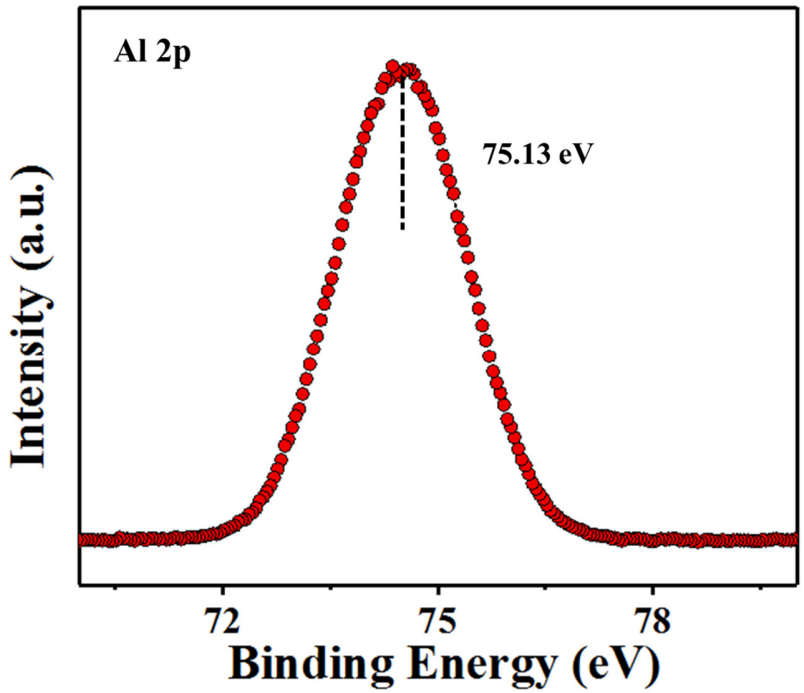

Figure S4. High resolution XPS profile for the Al 2p core level of the Al_2O_3 thin film by ALD.

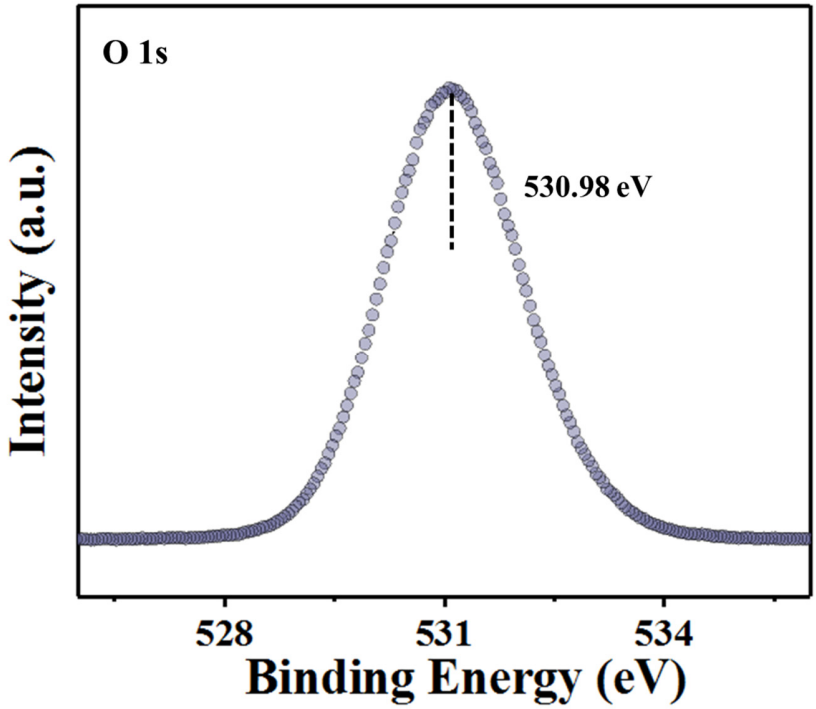

Figure S5. High resolution XPS profile for the O 1s core level of the Al_2O_3 thin film by ALD.

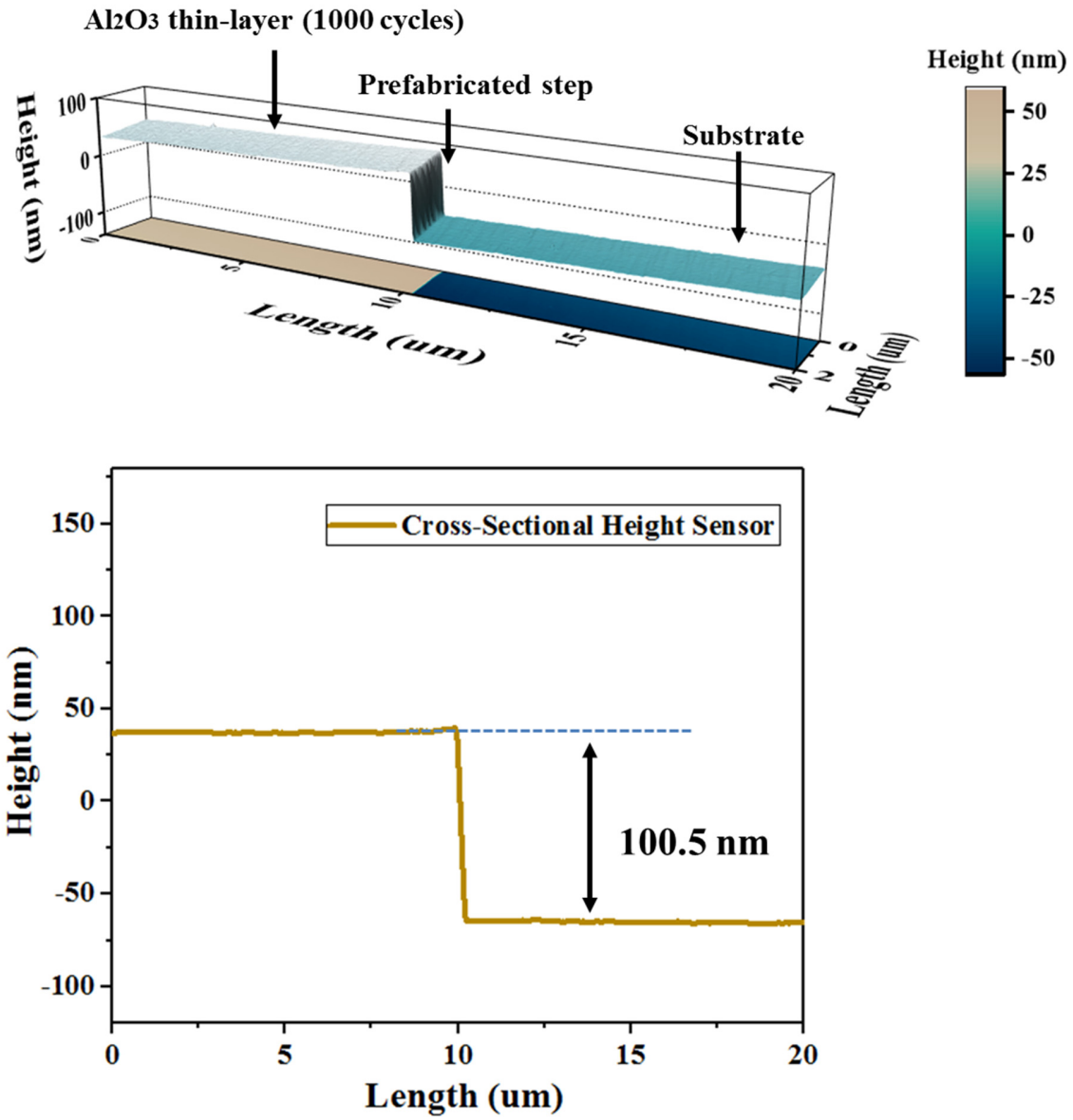

Figure S6. Height measurement performed for 1000 cycles of Al_2O_3 thin-layer, where a steep and clear step was made at the edge of the Al_2O_3 thin-layer by applying a mask to the local area of the substrate during deposition. (up) 2×20 μm^2 AFM image of the prefabricated step and (down) the corresponding height line-scan across the step.

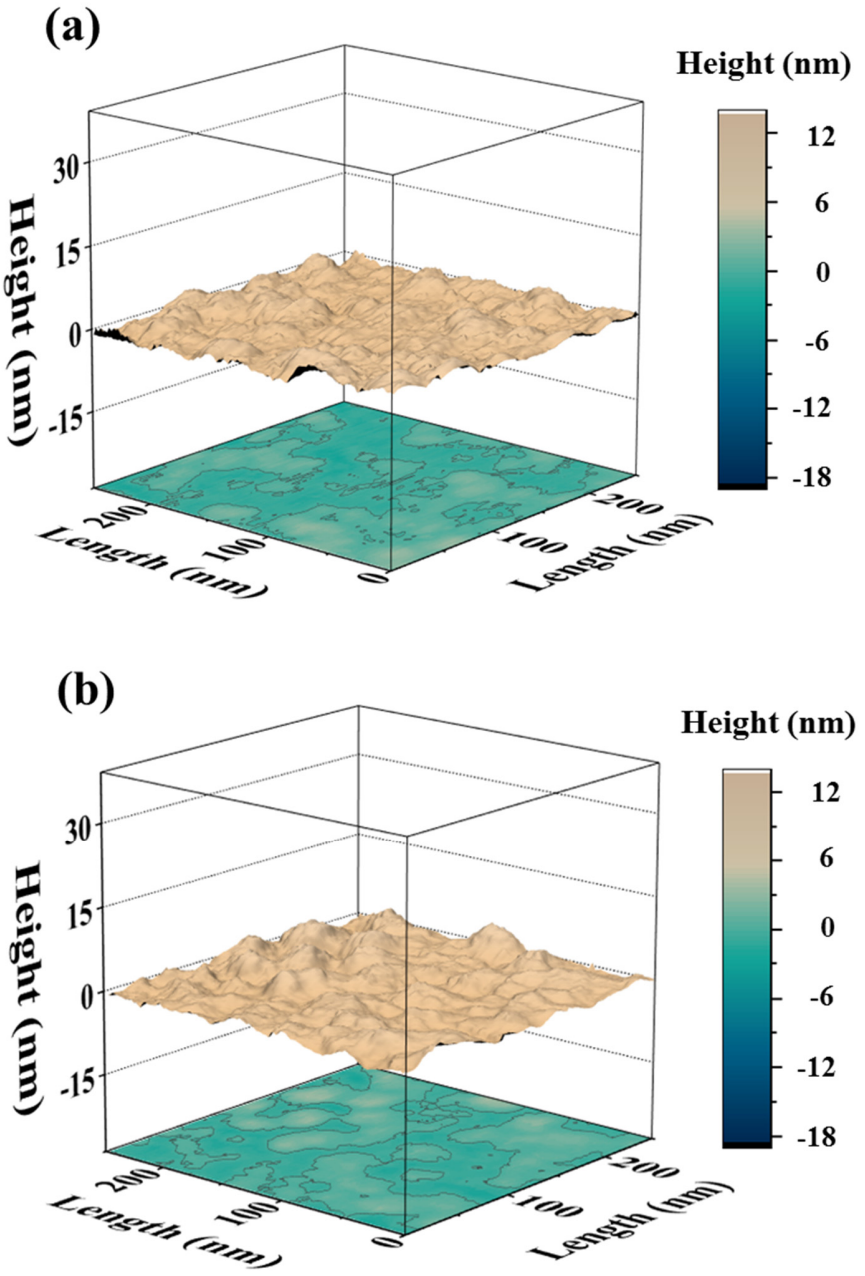

Figure S7. AFM images of surface morphology for (a) 200nm AZ-NLs and (b) 600nm AZ-NLs, with a root-mean-square (RMS) roughness of 0.92 nm and 1.03 nm, respectively.

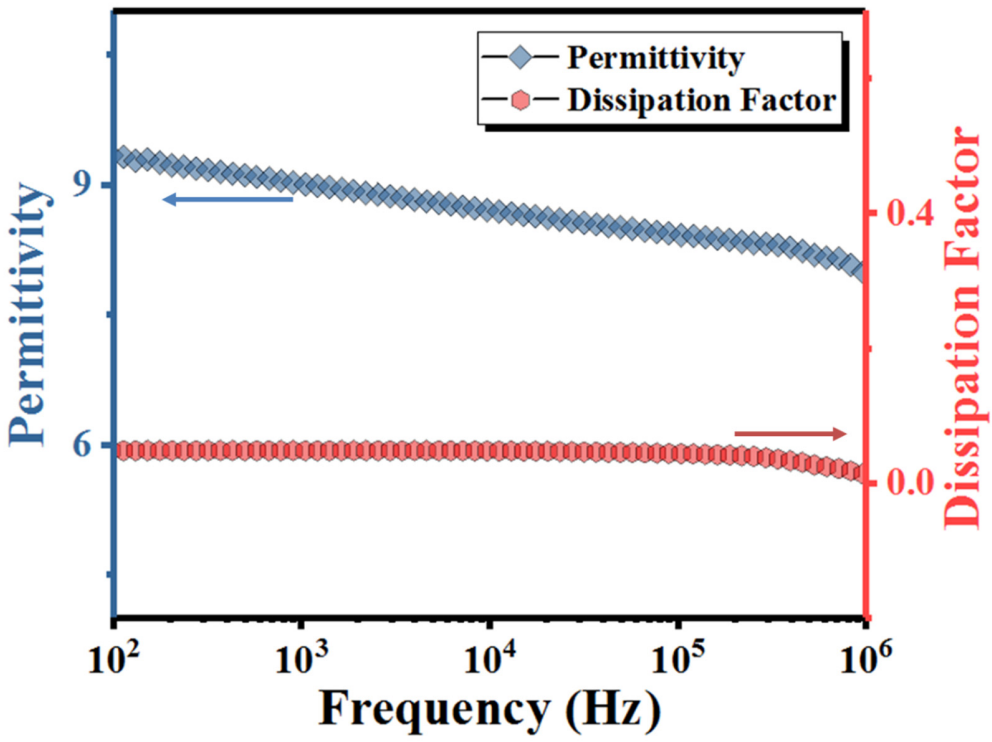

Figure S8. Frequency dependences of permittivity and dissipation factor measured at room temperature for Al_2O_3 single film by ALD.

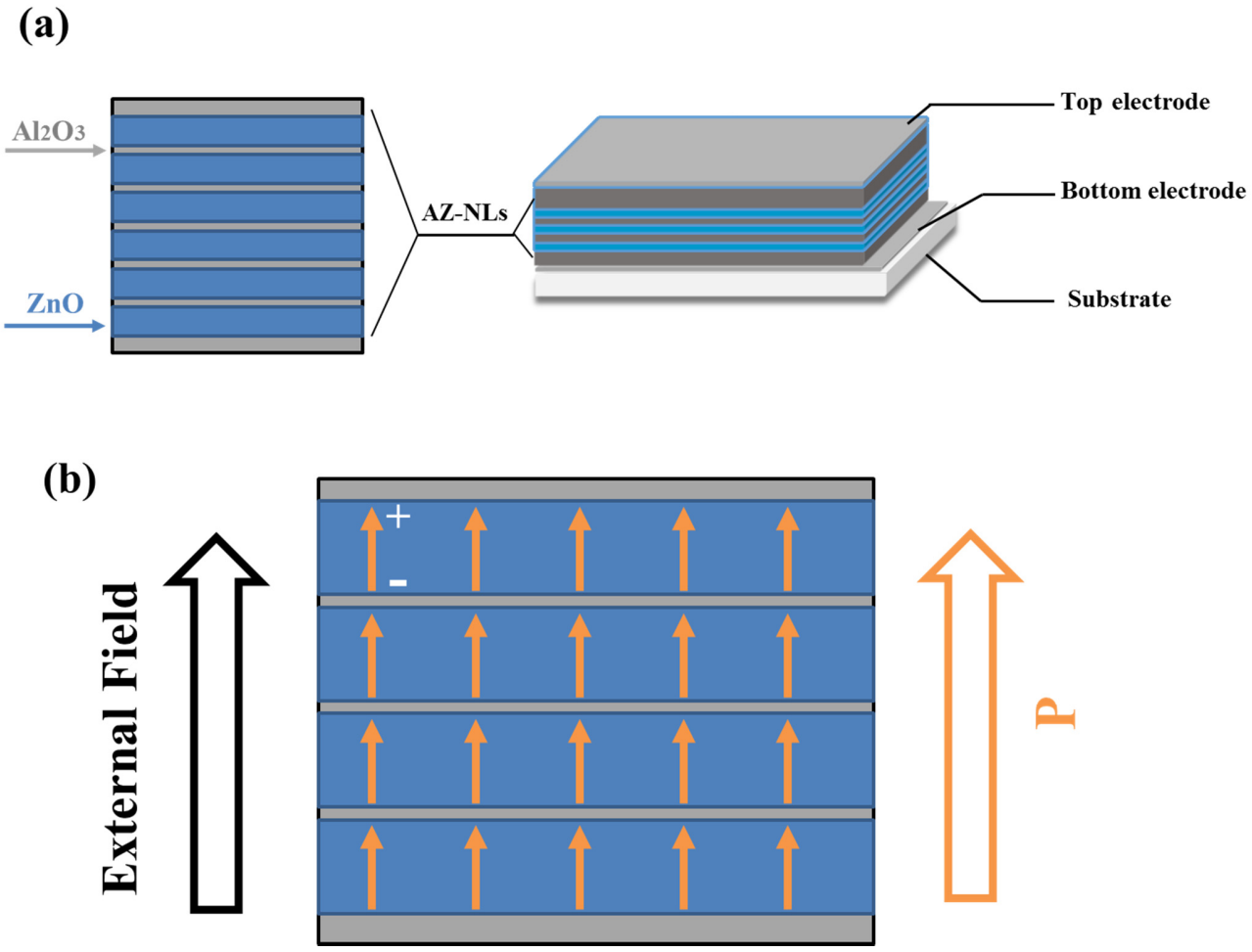

Figure S9. (a) The schematic structure of AZ-NLs based capacitors. (b) Polarization of the AZ-NLs under external field.

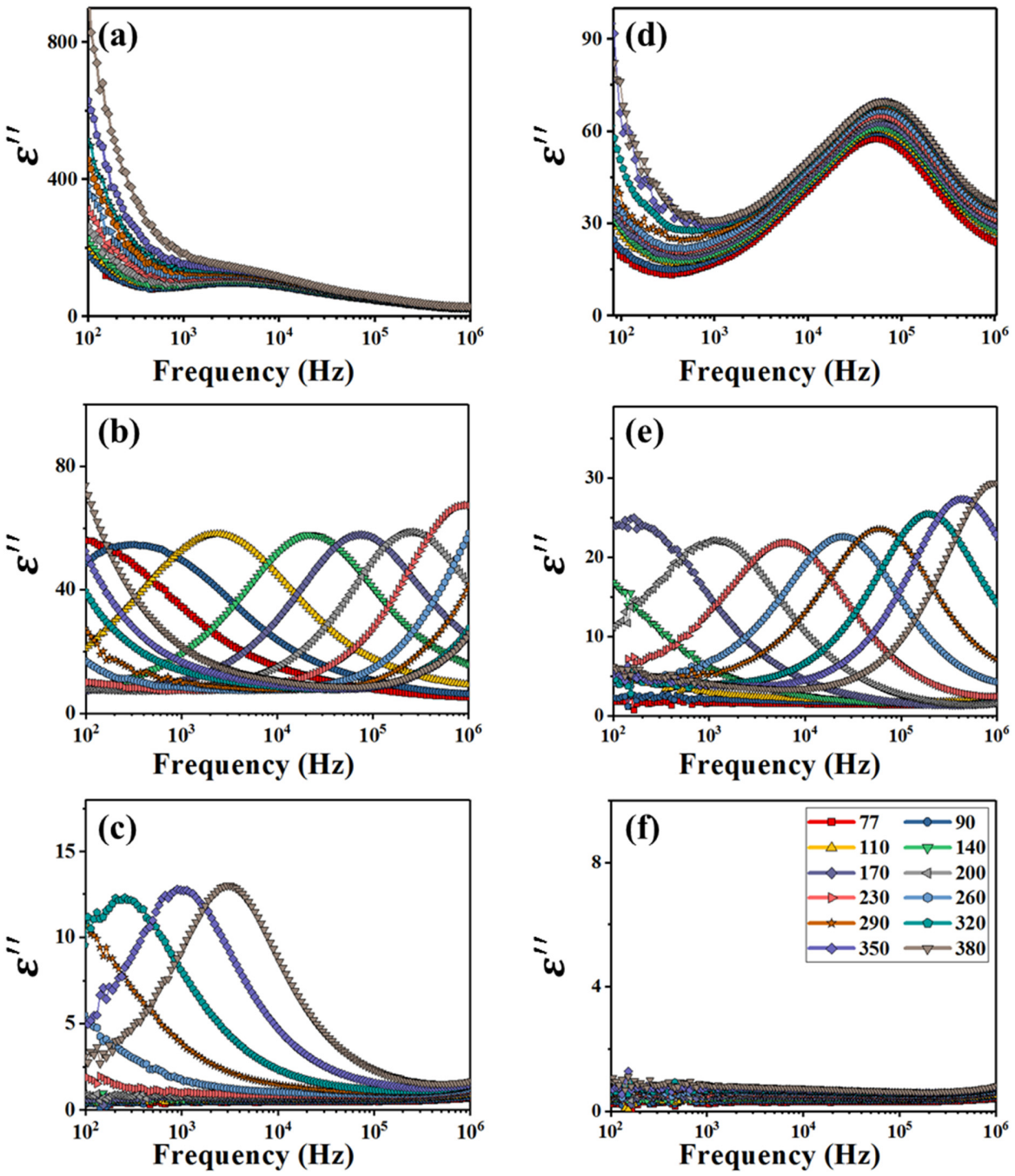

Figure S10. Dielectric loss spectra for (a) 10a-40z, (b) 10a-20z, (c) 10a-14z, (d) 10a-10z, (e) 10a-8z and (f) 10a-6z AZ-NLs measured at different temperatures from 77 to 380K.

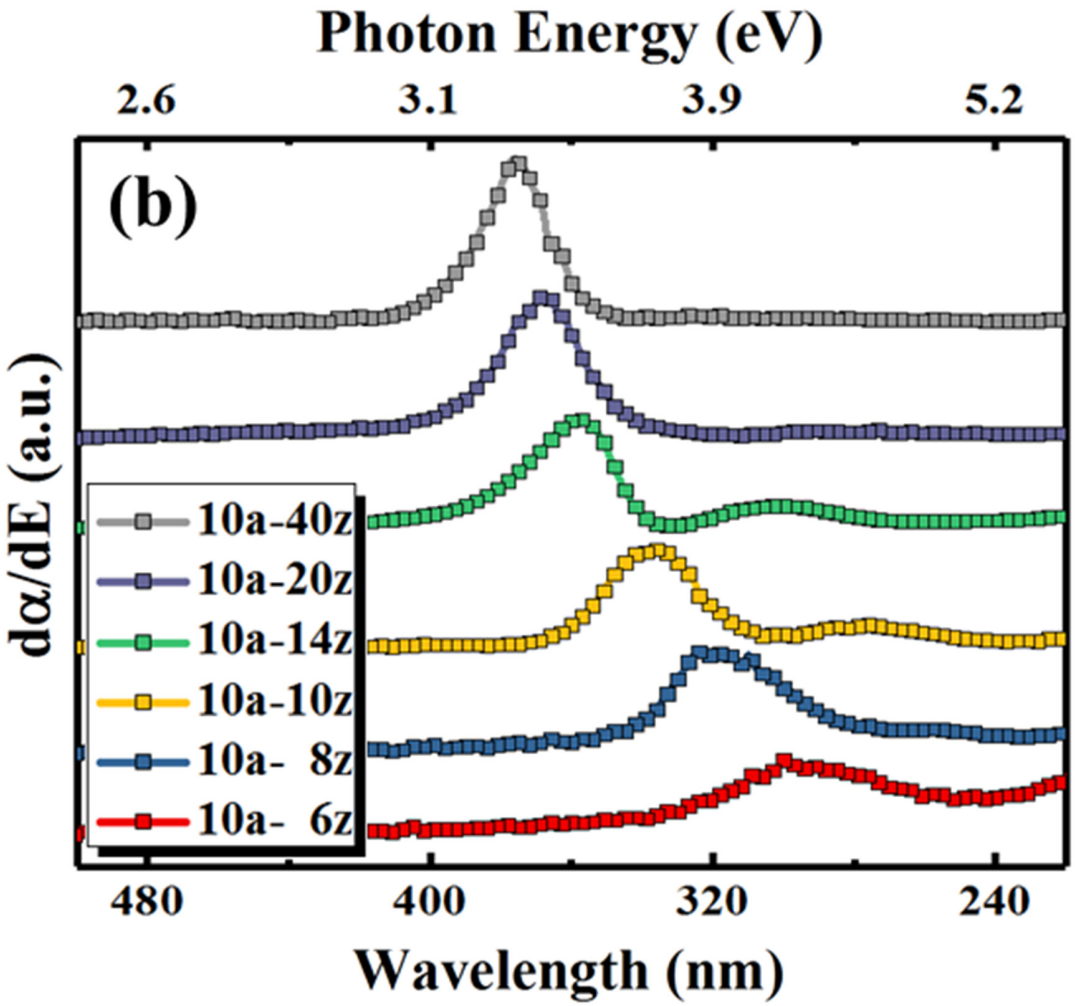

Figure S11. The derivative of absorption to photon energy dα/dE profiles of the AZ-NLs, with W_{ZnO} decreasing from 40 to 6 cycles, where the peak on each curve indicates the optical bandgap.

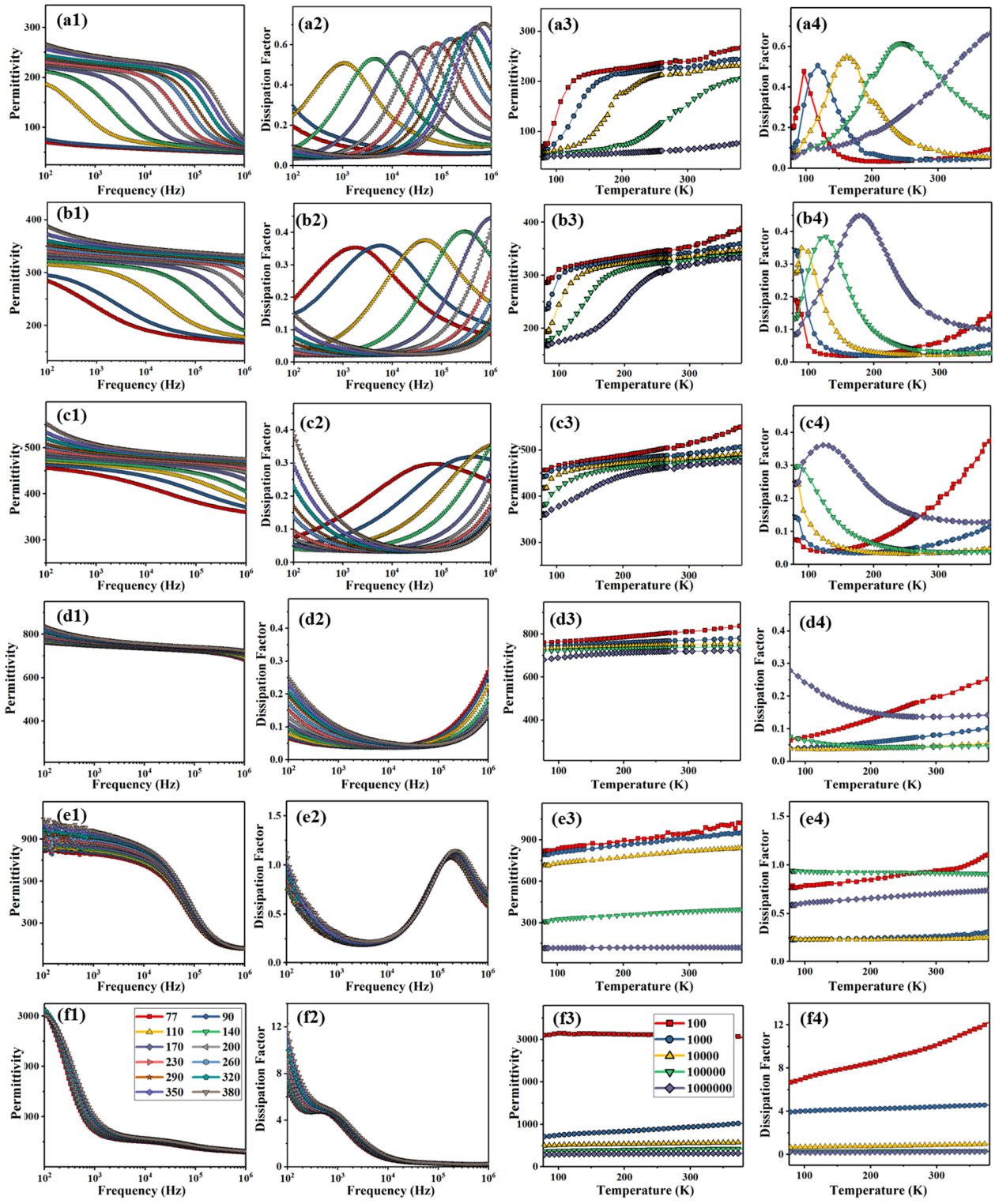

Figure S12. Dielectric performances of (a) 14a-14z, (b) 8a-14z, (c) 6a-14z, (d) 4a-14z, (e) 2a-14z and (f) 1a-14z AZ-NLs, where (1) and (2) are frequency spectra of permittivity and

dissipation factor measured at different temperatures ranging from 77 to 380K, (3) and (4) represent temperature-dependent permittivity and dissipation of selected frequencies. The legends for the frequency and the temperature spectra can be seen in (f1) and (f3), respectively.

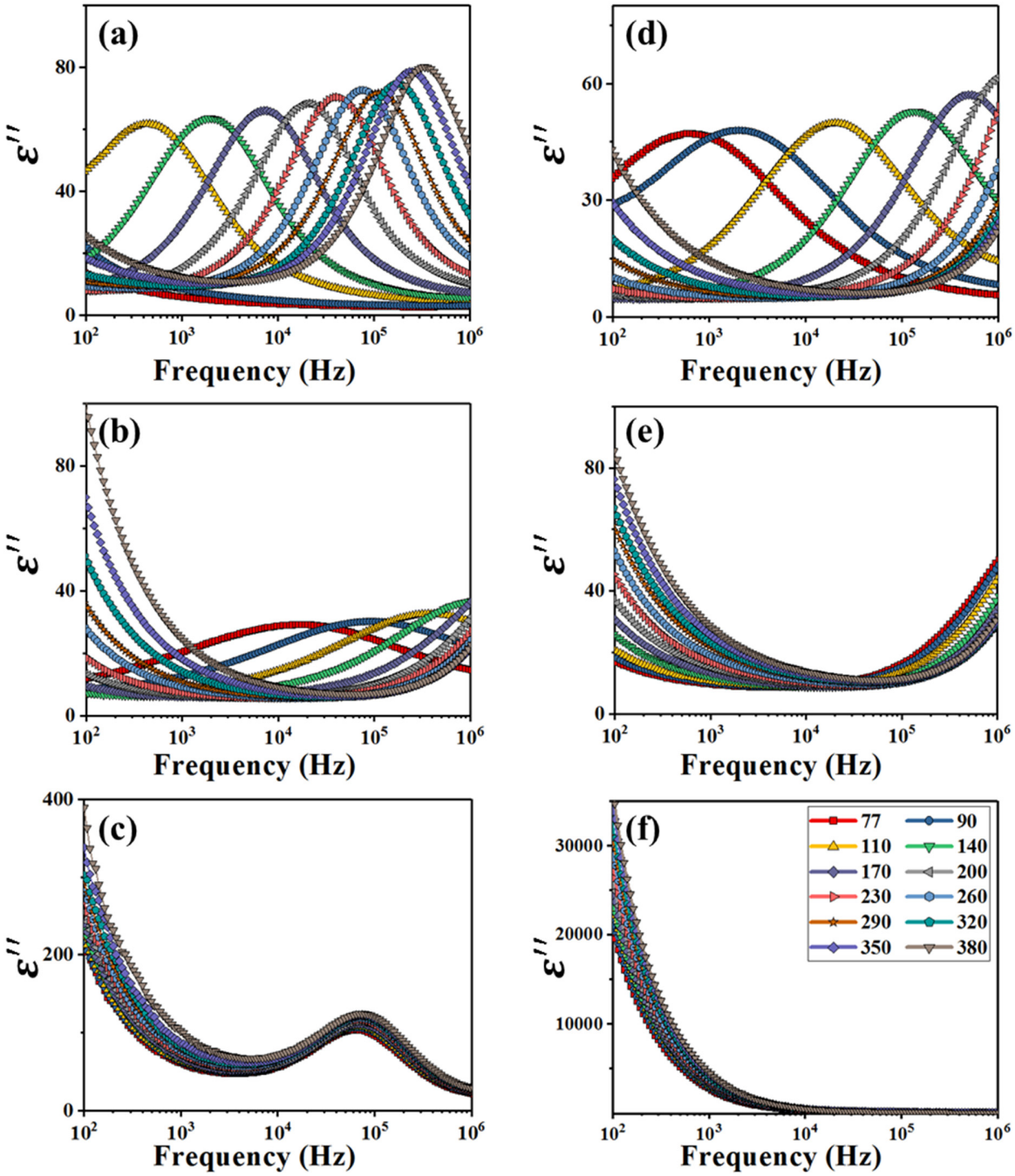

Figure S13. Dielectric loss spectra for (a) 14a-14z, (b) 8a-14z, (c) 6a-14z, (d) 4a-14z, (e) 2a-14z and (f) 1a-14z AZ-NLs measured at different temperatures from 77 to 380K.

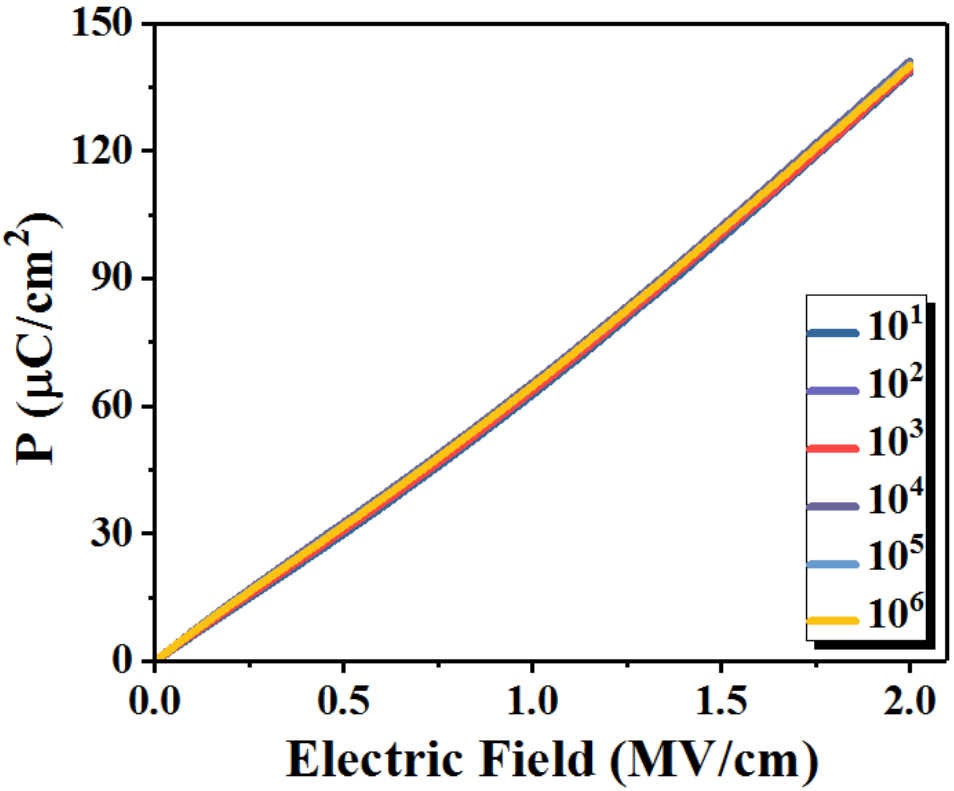

Figure S14. P−E loops for 4a-14z AZ-NLs during the fatigue process up to 1×10^6 cycles at 2.0 MV/cm.